Analysis of an Image-Based Method to Quantify the Size and Shape of Sand Particles

F. Altuhafi[1]; C. O'Sullivan[2]; and I. Cavarretta[3]

Abstract: Sand response depends on particle morphology (size and shape). In geotechnical research and practice, size is typically assessed by sieve analysis and particle shapes are qualitatively described. Technological developments mean that digital images of sand particles can easily be obtained, enabling shape to be quantified. The complexity associated with many digital image analysis algorithms seems to have restricted their use to fundamental research studies. This study introduces a pragmatic approach for quantitative shape analysis that has the potential to be broadly adopted in geotechnical engineering research and practice. The approach generates three shape measures (convexity, sphericity, and aspect ratio) that can easily be calculated from digital images. Following an analysis of these shape measures and the imaging method used here, a database of 36 sands, including many of the sands commonly used in geotechnical research, is presented. The subjective nature of qualitative description is clear from the discrepancies that were found in published shape assessments of these sands. Convexity, sphericity, and aspect ratio data for each of the 36 sands are presented. The relevance of these parameters to geotechnical engineering is established by comparing them with widely used qualitative descriptions. **DOI: 10.1061/(ASCE)GT.1943-5606.0000855.** © *2013 American Society of Civil Engineers.*

CE Database subject headings: Shape; Size; Particles; Sand (soil type); Imaging techniques.

Author keywords: Shape; Size; Particles; Sand.

Introduction

Particle size, particle-size distribution, and particle shape are basic parameters used to describe sands. In most geotechnical engineering research and in industrial practice, sand sizes are measured using sieve analysis and particle shape is assessed qualitatively. Sophisticated quantitative, imaging-based methods have been proposed in the literature (Bowman et al. 2001; Sukumaran and Ashmawy 2001). Although these methods are useful for fundamental research, it appears that the level of complexity involved has hindered their routine use in material characterization. In this paper, a relatively simple, image analysis-based approach to characterize particle morphologies is analyzed. The method generates three shape measures: convexity, sphericity, and aspect ratio. Given its simplicity and the small number of parameters involved, this is a pragmatic method that is amenable to general sand characterization for both geotechnical research and practice.

Following a description and critical analysis of the new approach, a database giving quantitative shape data for 36 sands is presented. This database highlights the shortcomings of qualitative shape analysis by showing the lack of consensus among descriptions of a given type of sand. A transition toward using quantitative shape analysis as a basic characterization tool is most likely to be achieved if engineers can develop an understanding of the meaning of new shape parameters relative to their current practice. Therefore, correlations between the new method and established qualitative measures are explored.

[1]Postdoctoral Research Fellow, Dept. of Civil and Environmental Engineering, Imperial College London SW7 2AZ, London, U.K.

[2]Senior Lecturer, Dept. of Civil and Environmental Engineering, Imperial College London, London SW7 2AZ, U.K. (corresponding author). E-mail: cath.osullivan@imperial.ac.uk

[3]Senior Lecturer, Dept. of Civil and Environmental Engineering Univ. of Surrey, Guildford GU2 7XH, U.K.

Note. This manuscript was submitted on September 5, 2011; approved on October 22, 2012; published online on October 24, 2012. Discussion period open until January 1, 2014; separate discussions must be submitted for individual papers. This paper is part of the ***Journal of Geotechnical and Geoenvironmental Engineering***, Vol. 139, No. 8, August 1, 2013. ©ASCE, ISSN 1090-0241/2013/8-1290–1307/$25.00.

Background

Particle-Size Distribution

Particle size determines the soil type. The distribution of particle sizes influences soil response characteristics, including the angle of shearing resistance (Holtz and Kovacs 1981), compressibility (Yang 2006), and susceptibility to internal erosion (Kenney and Lau 1985). Traditionally, standard sieves [according to the British Standards Institute (1997) or equivalent international code] are used. Sieving gives no information on the particle-size distributions between the sieve intervals; additional shortcomings of sieving are listed in Allen (1997).

Alternative methods to determine sand particle size are available (e.g., laser diffraction or single particle optical sizing), as considered by McCave and Syvitski (1991), Abbireddy and Clayton (2009), White (2003), and Rhodes (2000). Mechanical automation of microscope stages allows statistically representative numbers of particles to be considered. However, these microscopy-based methods involve analysis of two-dimensional (2D) images, and therefore they suffer from the disadvantage that the minor principal axis of the particle is vertical when the particle is at rest in its most stable position (Abbireddy and Clayton 2009; Cavarretta 2009). Three-dimensional (3D) geometrical data can be obtained using advanced optical microscopy [e.g., *Axiovision's* topography module (Zeiss 2007) or microcomputed tomography (Fonseca 2011)]. However, the complexity of these methods limits their use to fundamental research.

Particle Shape

Particle shape influences the mechanical response characteristics of sand. The density and range of attainable void ratios vary with shape

(Mitchell and Soga 2005; Cho et al. 2006; Pestana and Whittle 1995; Rouse et al. 2008). Stiffness is also shape-dependent (Cho et al. 2006; Pestana and Salvati 2006). Cho et al. (2006) demonstrated relationships between shape and various critical state soil mechanics parameters. Clayton et al. (2006) found that shape influences the amount of degradation under cyclic loading. Numerous other research studies documenting the influence of particle geometry on sand response can be found in the literature, and therefore a robust means to quantify sand particle shapes is needed. Clark (1981) gives examples of a number of approaches for quantifying particle shape in geomechanics and geology. Shape classification schemes should ideally use descriptors that can independently describe particle form, roundness, or surface texture (Barrett 1980; ISO 2008; Cavarretta 2009). In soil mechanics, particle geometry is commonly described in terms of roundness and sphericity.

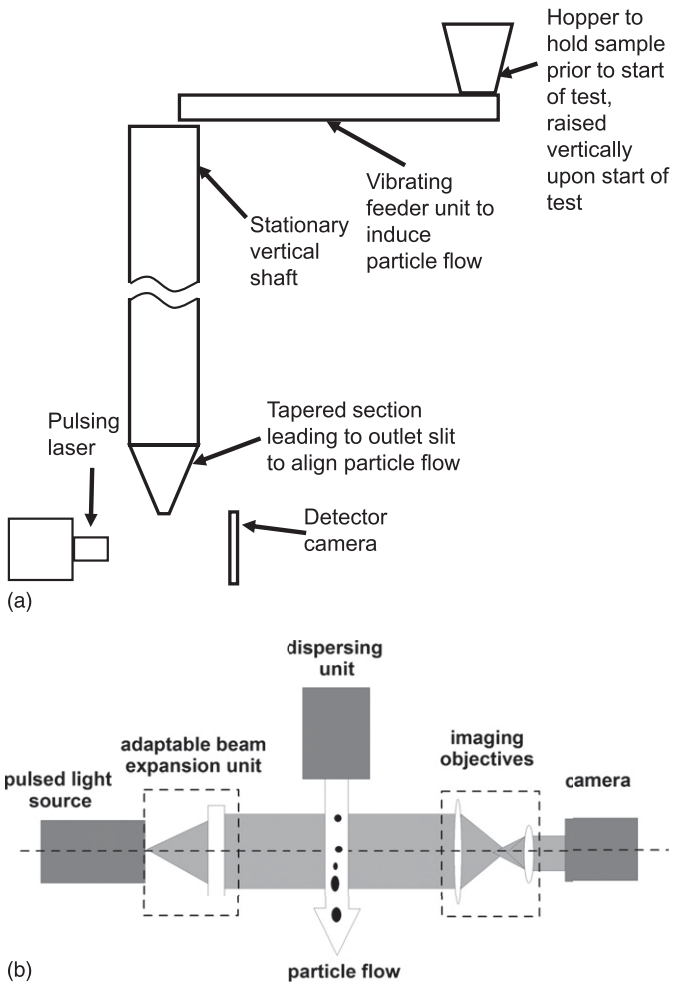

Fig. 1. Overview of the QICPIC apparatus

Roundness is calculated by considering the projected outline of a particle on a plane and taking the mean of the ratio r_i/R_o of the individual corners, where r_i is the radius of the curvature of corner i, and R_o is the radius of the maximum inscribed circle (Wadell 1932). Accurate identification of a corner and determination of the roundness is nontrivial, and the parameter is scale dependent (Chan 2007; Cavarretta 2009). However, although some authors (Cho et al. 2006; Rouse et al. 2008) provide numerical roundness values, in geotechnical research (Cavarretta et al. 2010), authors typically describe roundness qualitatively. In fact, in most documented research studies, particle shape description follows the approach proposed by Youd (1972) and D2488 (ASTM 1990) and particles are classified according to seven classes of roundness to be very angular, angular, angular/subangular, subangular, subrounded, rounded, and well rounded. The origin of this system may be the chart provided by Powers (1953).

Sphericity is a measure of form, and it quantifies the degree of similarity between a particle and a sphere. There is not a consensus as to what exactly is meant by the term sphericity in geomechanics, and various definitions available are discussed by Mitchell and Soga (2005) and Alshibli and Alsaleh (2004). Wadell (1932) defined sphericity to be the ratio between the surface area of the sphere of the same volume to the actual surface area of the particle. The practical difficulty in calculating the surface area of the irregular-shaped particles is solved by the provision of a reference chart by Krumbein and Sloss (1963). In their chart, Krumbein and Sloss used class intervals of 0.2 and placed reference images with values of sphericity (S^{KS}) and roundness (R^{KS}) into appropriate bins. Krumbein and Sloss reported that S^{KS} was related to the "proportion between length and breadth of the particle" and that roundness was related to the curvature of the outlines. The Krumbein and Sloss chart was used by Cho et al. (2006), who proposed averaging the roundness and sphericity values to get a new parameter called the regularity, ρ. Cho et al. (2006) quantified sphericity to be the ratio of "diameter of the largest inscribed sphere" to the "diameter of the smallest circumscribed sphere."

Digital silhouettes of particles can be obtained by processing 2D images obtained using conventional digital photography, optical microscopy, or from thin sections. Various shape characterization algorithms can be applied to these silhouettes. This approach, in principle, has some advantages over visual comparison with the Krumbein and Sloss (1963) chart; the analysis is less user-subjective and less tedious, allowing a more accurate assessment of a larger number of particles. However, there will always be a bias in the orientation, therefore a true assessment of 3D particle shape requires additional measurements (e.g., use of a motorized microscope stage and specialized image analysis software). Obtaining images of large numbers of particles, so that the measured shapes are statistically representative, has been challenging.

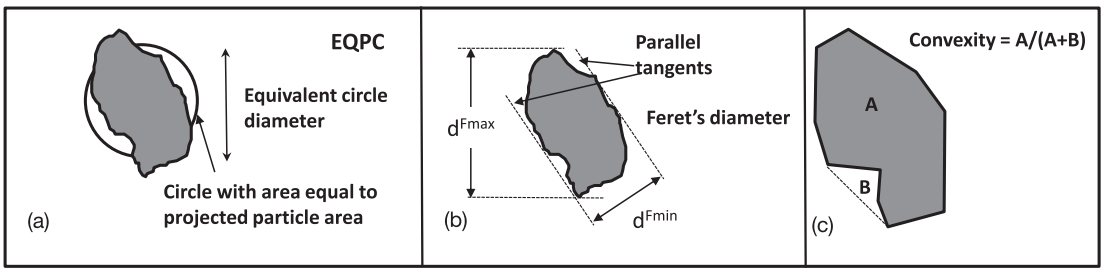

Fig. 2. Definitions of particle shape and size considered

J. Geotech. Geoenviron. Eng. 2013.139:1290-1307.

Overview of the QICPIC Apparatus

The QICPIC imaging system was developed by Sympatec GmBH for use on particles sized between 1 μm and 30 mm (Sympatec 2008; Witt et al. 2004). For clarity, the key principles are summarized here, and consideration is restricted to sand particles > 100 μm and the dry dispersion system. For particles < 100 μm, wet dispersion is recommended. An overview of the system is given in Fig. 1(a). Initially, the sample is placed in a hopper. At the start of the test, the hopper is raised by a user-defined height, h, ($0.5 < h < 15$ mm), and a controlled vibration of the feeding unit generates a relatively steady flow of particles and adds kinetic energy to the particles before they fall into the vertical shaft. As illustrated in Fig. 1(b), the particles pass between a specially configured light source and a pair of imaging lenses configured to minimize focusing problems. This light/laser source exposure time is less than 1 ns, and therefore the image blur is minimized. The camera records a sequence of binary images (frames) of the particles. The camera detector operates at up to 450 frames per seconds, and therefore a statistically representative number of particles can be considered in a short span of time.

As the particles fall through the shaft, particle-to-wall collisions and particle-to-particle collisions create a smooth dispersion with minimal overlap in the images generated. A vacuum-extraction unit placed at the bottom of the system (a vacuum cleaner) generates a downward flow of air through the shaft. An outlet slit placed at the end of the shaft aligns the particle flow for imaging beneath its opening. The combination of vibration, collisions, and use of a vacuum minimizes the tendency for preferential alignment of the particles. Each particle is usually depicted in different positions in subsequent frames, and the random orientation of particles during imaging was confirmed by careful visual examination of the images themselves.

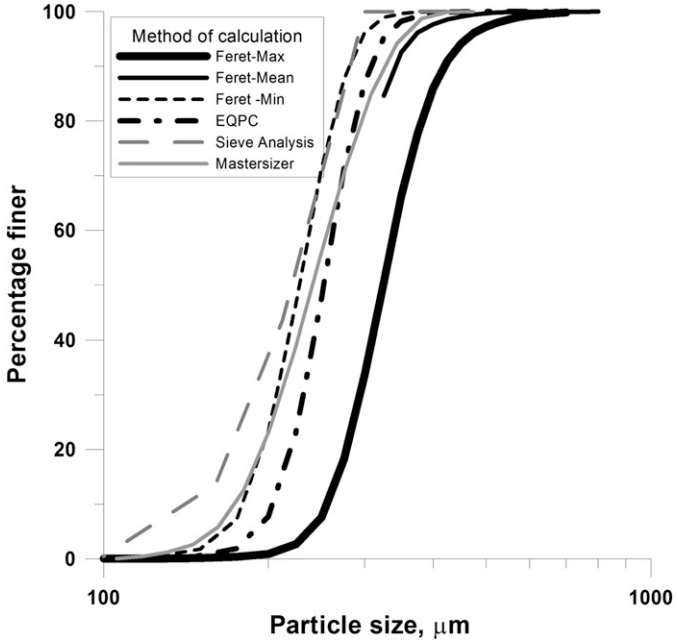

Fig. 3. Comparison of size distribution data for Toyura Sand

Theoretically, the approach used overcomes the restriction of conventional optical analysis where the particle image plane is orthogonal to the shortest axis of the particle and therefore a more realistic measure of true 3D shapes can be attained. Using this approach, statistically representative numbers of particles can be imaged relatively quickly; the number of particles required to generate repeatable, representative results depends on the particle-size distribution. The minimum number of particles required will depend on the particular sand, and simple repeat tests and parametric studies should be carried out for each material considered to assess whether the sample size is adequate. Joudi (2008) considered a number of sands with a variety of particle-size distributions, all having d_{50} values between 160 and 350 μm and showed that 5 g is an adequate amount of sample for sands having these sizes.

Propriety software is used to obtain distributions of particle size and shape. It is possible to filter the data, and because the pixel size for the dry dispersion unit is 10 μm, particles smaller than 100 μm were excluded from consideration. The analysis of the resulting images uses measures that are implemented in a number of available imaging software packages [e.g., *Axiovision* (Zeiss 2007), *ImageJ* (Schneider et al. 2012), *MATLAB* (MathWorks 2011)]. Thus, although the data considered were generated using the QICPIC apparatus, it is straightforward to apply the analysis approaches used to binary images of particles obtained using other imaging approaches.

Particle-Size Distribution

In geomechanics, particle-size distributions are usually measured using sieve analysis (denoted d^{sieve} here); therefore, whereas sieve data are subject to limitations, as previously noted, they provide a useful reference to establish the applicability of the image-based approach to measure particle size. Several particle size measures are directly available within the QICPIC system. Referring to Fig. 2(a), the measure d^{EQPC} is the diameter of a circle whose area equals the projected area of the particle, and is arguably the best measure of the overall particle size. A Feret diameter can also be measured [Fig. 2(b)]; this is the distance between two tangents on opposite sides of the particle. The maximum, minimum, and mean Feret diameters are being given by $d^{F\text{max}}$, $d^{F\text{min}}$, and $d^{F\text{mean}}$, respectively. Feret diameters vary much more with irregular-shaped particles than

Table 1. Comparison of Median Particle size (d_{50}) and Coefficient of Uniformity (U) for QICPIC, Mastersizer, and Sieve Data

Sand	$d_{50}{}^{\text{sieve}}$ (μm)	$d_{50}{}^{\text{mastersizer}}$ (μm)	$d_{50}{}^{ECQP}$ (μm)	$d_{50}{}^{F\text{min}}$ (μm)	U^{sieve}	$U^{\text{mastersizer}}$	U^{ECQP}	$U^{F\text{min}}$
Fontainebleau	249	—	258	230	1.7	—	1.5	1.43
Badger	805	—	977	882	1.3	—	1.1	1.2
Toyoura	222	241	251	228	1.7	1.48	1.3	1.3
Leighton Buzzard	765	—	823	762	1.6	—	1.3	1.3
Frasier River	273	252	356	300	1.7	1.9	1.6	1.67
Hostun	364	422	423	380	2.0	1.6	1.5	1.54
Reigate	241	—	299	272	1.9	—	1.5	1.55
Ottawa Fine	378	—	481	406	1.8	—	1.4	1.46
Ottawa Coarse	798	—	859	777	1.3	—	1.2	1.18
Thames Valley	237	—	250	243	2.2	—	1.8	1.8

J. Geotech. Geoenviron. Eng. 2013.139:1290-1307.

with regular shapes, and consequently the maximum and minimum can be considerably larger and smaller than the d^{EQPC}.

Fig. 3 compares the particle-size distributions for Toyoura Sand obtained using these different size measures with sieve analysis and laser diffraction (using a Mastersizer LS100). There are clear differences in the sizes obtained, considering the extreme $d_{50}^{F\max} = 325\mu$m and $d_{50}^{F\min} = 228\mu$m. Although the sieve data represent a lower bound to the measurements, they are similar to the the $d^{F\min}$ data for the largest 50% (by volume) of particles in the system. The d^{EQPC} values are consistently slightly smaller than the $d^{F\text{mean}}$ values. Table 1 summarizes a comparison of the particle-size distributions for a range of sands, considering d^{sieve}, $d^{\text{mastersizer}}$, d^{EQPC}, and $d^{F\min}$ data to calculate the median particle diameters (d_{50}^{sieve}, $d_{50}^{\text{mastersizer}}$, d_{50}^{ECQP}, $d_{50}^{F\min}$) and the coefficients of uniformity (U^{sieve}, $U^{\text{mastersizer}}$, U^{ECQP}, $U^{F\min}$). The data presented in Fig. 3 and Table 1 indicate that, of the available methods, $d^{F\min}$ is the size measure that most closely corresponds with sieve data, and the similarity between the size measures depends on the sand type. No definite conclusion can be made about which size measure correlates best with the Mastersizer data.

The relationship between the d^{sieve} and $d^{F\min}$ values can, to some extent, be understood by considering the schematic diagram of a particle falling through a sieve opening in Fig. 4. The particle considered here has a ratio of the minor to intermediate dimension of about 0.65. In both Figs. 4(a and b), the longest dimension of the particle is orthogonal to the sieve opening. The particle is not restricted to fall with its intermediate axis parallel to one of the sieve sizes; under the action of the energy input during sieving, the particle can reorientate to be at an angle to the sieve sides. The sieve size through which the particle will pass is therefore dependent on both the intermediate and minimum (minor) particle dimensions.

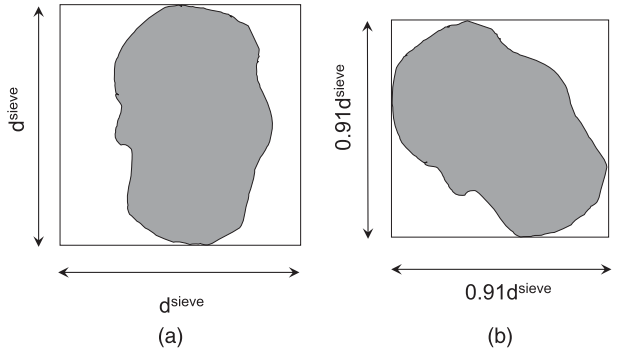

Fig. 4. Consideration of particle orientation relative to sieve opening

Aspect Ratio, Convexity, and Sphericity Values for Sands

The inbuilt shape measures used in the QICPIC system are the aspect ratio (AR), the convexity (Cx), and the sphericity (S^{QP}). The Feret diameters are used to define the aspect ratio and $\text{AR} = d^{F\min}/d^{F\max}$. Referring to Fig. 2(c), convexity, Cx, is the ratio between the imaged particle area (A) and the area of the convex hull ($A + B$). The convexity is a measure of the compactness of a particle. The sphericity measure available within the QICPIC system is denoted S^{QP}, and $S^{QP} = 2\sqrt{\pi A}/P$, where A is the projected area of the particle, P is the projected perimeter, and $2\sqrt{\pi A}$ is the perimeter of a circle whose area equals the projected particle area. These definitions can be easily applied to any binary images of particles, and therefore, even without access to the QICPIC system, geotechnical engineers can use these quantitative measures of shape.

To gain understanding of the meaning of the QICPIC shape measures for sand grains, the widely used reference chart proposed

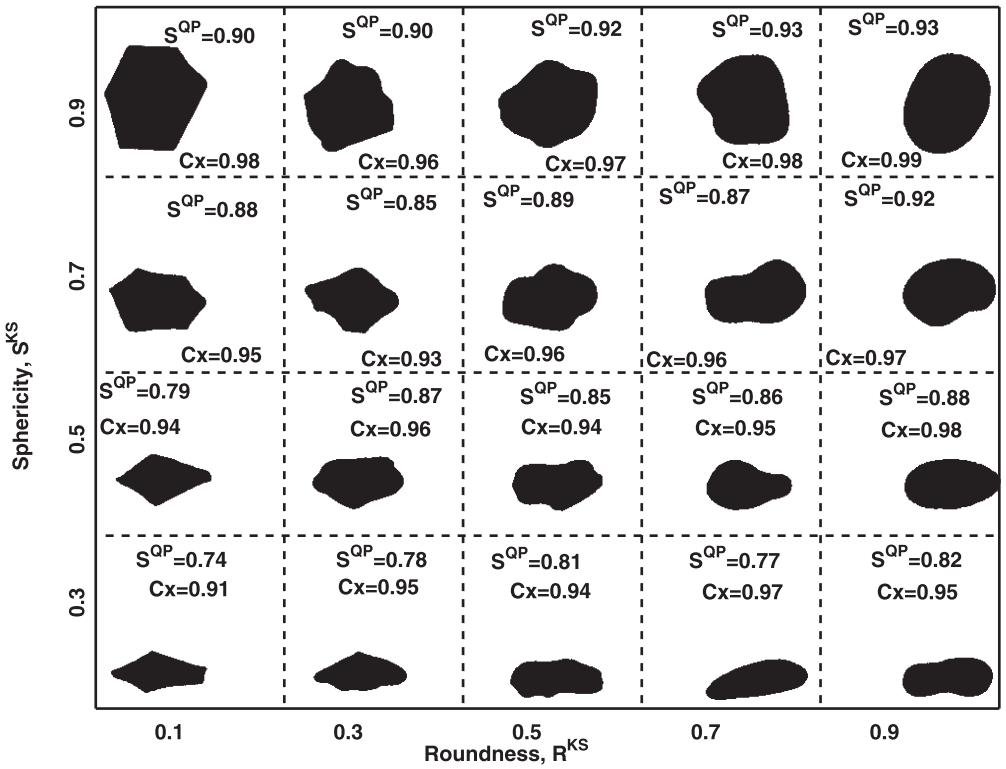

Fig. 5. Sphericity (S^{QP}) and convexity (Cx) values for the reference particles considered by Krumbein and Sloss (1963)

J. Geotech. Geoenviron. Eng. 2013.139:1290-1307.

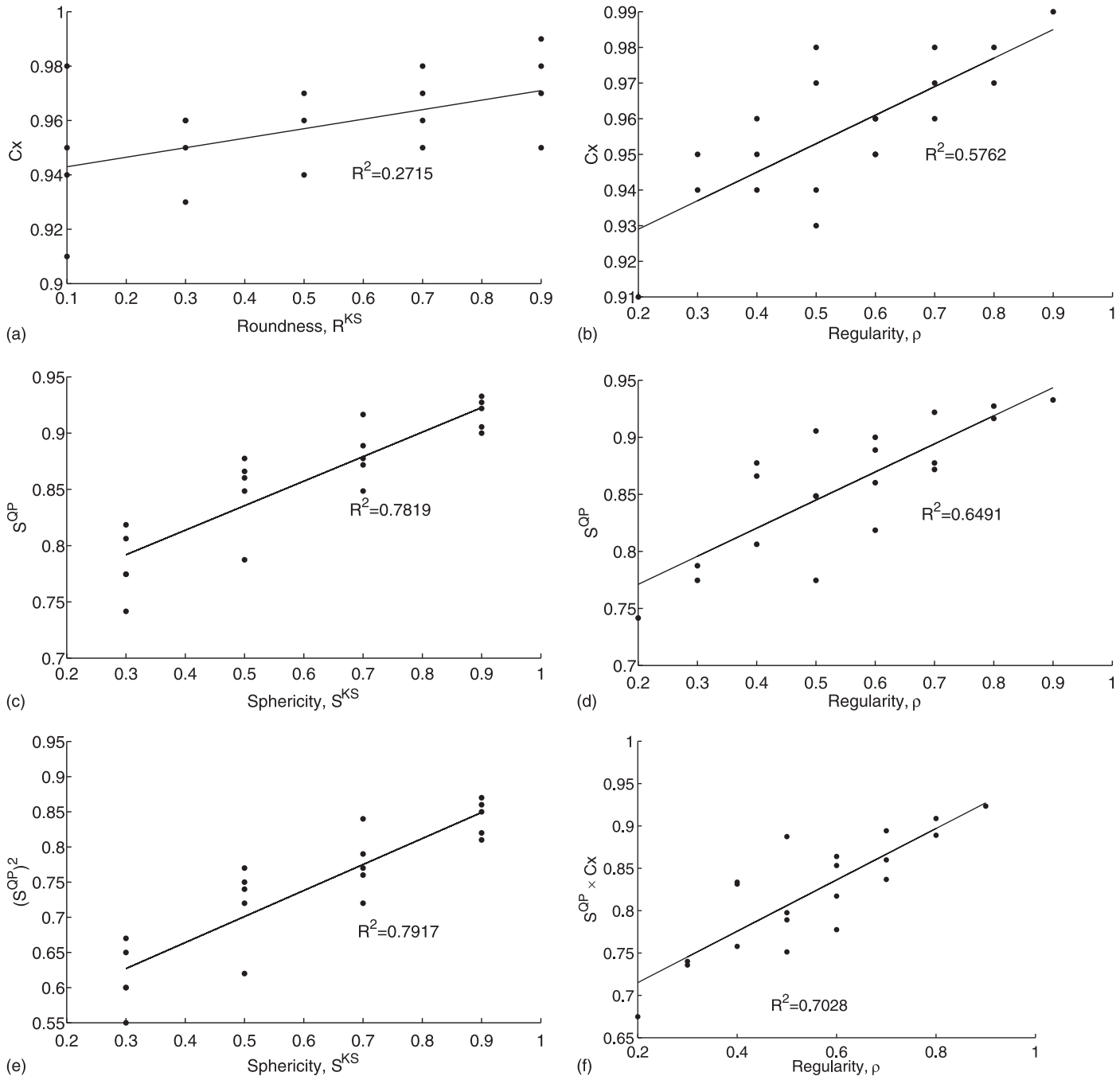

Fig. 6. Comparison of QICPIC shape metrics with measures of roundness, sphericity, and regularity for the reference particles considered by Krumbein and Sloss (1963)

by Krumbein and Sloss (1963) and used by Cho et al. (2006) was analyzed. Sukumaran and Ashmawy (2001) compared their shape and angularity factors with sphericity and roundness, as defined by Wadell (1932). The Krumbein and Sloss chart gives 20 images of sand grains, as illustrated in Fig. 5. Each of the 20 reference images was digitized and analyzed using the *Axiovision* software (Zeiss 2007) to get the radii of the maximum and minimum circumcircles ($r_{i,\max}$, $r_{c,\max}$) and values of $d^{F\min}$ and d^{FL}, where d^{FL} is the Feret diameter that is measured orthogonal to $d^{F\min}$. The aspect ratio, AR, was then calculated as $d^{F\min}/d^{FL}$. This definition gives values of the aspect ratio within 5% of those calculated using $d^{F\min}/d^{F\max}$ (Cavarretta 2009), and because it was easier to measure, it was used in the analysis of the Krumbein and Sloss chart. The *MATLAB* image analysis toolbox (MathWorks 2011) was used to determine the areas and perimeters of the outlines and the area of the convex hull. The image analysis involved was significantly simpler than use of the Fourier descriptor method (Fonseca and O'Sullivan 2008) or implementation of Wadell's definitions (Chan 2007).

The Cx and S^{QP} values calculated for each particle are given in Fig. 5, and both Cx and S^{QP} increase with R^{KS} and S^{KS}. Quantitatively, the Cx values do not correlate linearly with R^{KS} [$R^2 = 0.272$, Fig. 6(a)] or S^{KS} ($R^2 = 0.319$), but the correlation with ρ is slightly stronger [$R^2 = 0.576$, Fig. 6(b)]. There is a relatively clear correlation between S^{KS} and S^{QP} [$R^2 = 0.782$, Fig. 6(c)], and there is no

J. Geotech. Geoenviron. Eng. 2013.139:1290-1307.

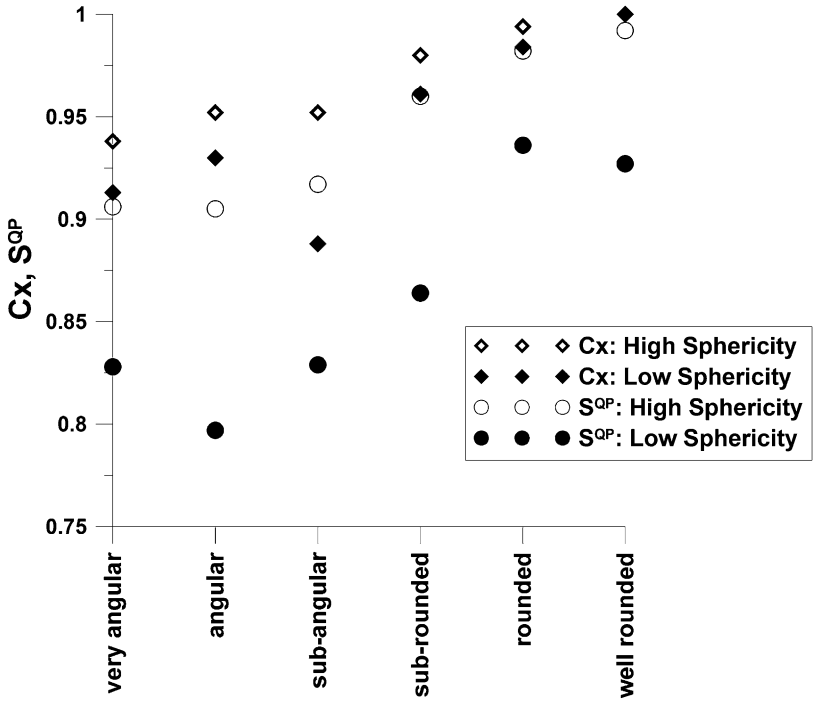

Fig. 7. Comparison of QICPIC shape metrics with qualitative measures of roundness and sphericity given in the reference chart of Powers (1953)

obvious correlation between the S^{QP} values and roundness; consequently, the apparent correlation between the S^{QP} values and regularity [Fig. 6(d)] develops only because of the S^{KS}:S^{QP} correlation. [Interestingly, there is an even stronger correlation between $(S^{QP})^2$ and ρ, with $R^2 = 0.792$.] Fig. 6(f) indicates that the product $S^{QP} \times Cx$ correlates better with regularity than either S^{QP} or Cx; however, the correlation is not sufficiently strong to allow these values to be used to predict the regularity.

The chart proposed by Powers (1953) was also digitized, and the QICPIC shape metrics were calculated for each reference particle. Referring to Fig. 7, there is generally a systematic increase in both Cx and S^{QP}, as the geometry evolves from being highly angular to being well-rounded. The Cx and S^{QP} values for the high-sphericity particles are consistently higher than those for the low-sphericity particles. [The exceptions to the trend have unusual shapes, as discussed by MacLeod (2002).]

The meaning of the Cx and S^{QP} values can be appreciated by reference to Fig. 8, which is a plot of representative silhouettes of natural particles for a range of natural sands against their corresponding S^{QP} and Cx values. The figure indicates that those particles with higher Cx and S^{QP} are more rounded and are in agreement with the general conclusion made from Fig. 7.

Analysis of Image Resolution

The image pixel size is finite relative to the particle size, and therefore the effects of image resolution on the QICPIC shape metrics must be considered. Three representative sands: Leighton Buzzard Sand, Toyoura Sand, and Ube Masado Sand, an angular volcanic sand from Iceland (Hamlin 2009), were considered. Ten representative grains of each sand were imaged using a digital optical microscope (Labinski 2011). The digital images were converted to binary format, the pixel resolution of the images was gradually reduced, and the shape measures Cx, S^{QP}, and AR were calculated. The resultant data are presented in Fig. 9, with the particle

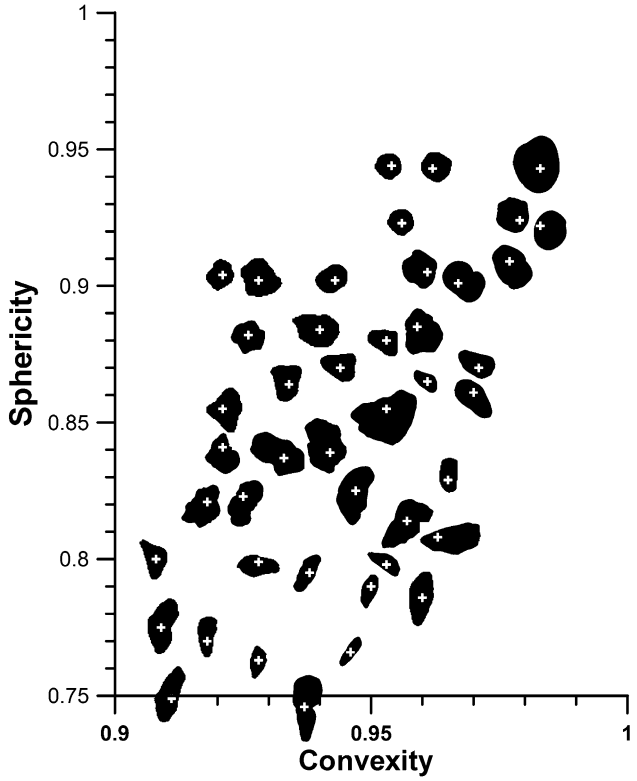

Fig. 8. Binary images for sand particles to illustrate representative geometries obtained for particles with $0.75 \leq S^{QP} < 1$ and $0.9 < Cx < 1$

size ($d^{F\min}$) being normalized by the pixel size and the error given by the difference between the shape measure for the highest resolution image and the current resolution, divided by the value for the highest resolution. The results are size dependent, and the error increases as the ratio of $d^{F\min}/(\text{pixel size})$ decreases. There is a lot of scatter in

J. Geotech. Geoenviron. Eng. 2013.139:1290-1307.

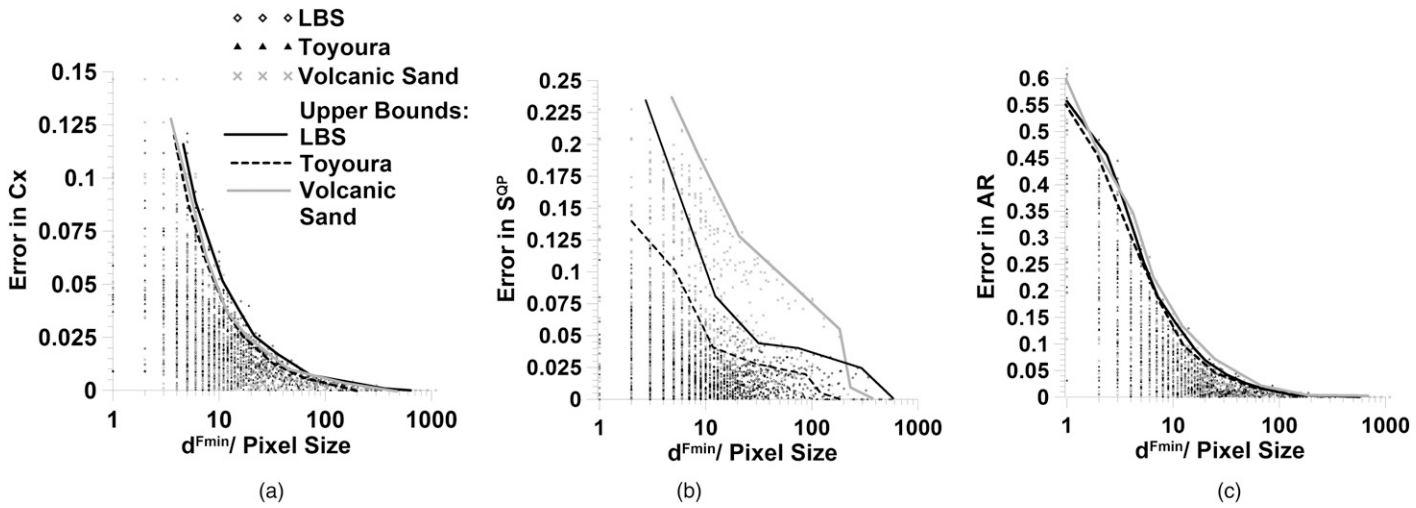

Fig. 9. (a) Plot of representative convexity (Cx_{50}) versus d_{50}; (b) plot of representative sphericity (S_{50}) versus d_{50}; (c) plot of representative aspect ratio (AR_{50}) versus d_{50}

the data, and envelopes indicating upper-bound estimates on the error are included in Fig. 9. The minimum value of the ratio $d^{Fmin}/(\text{pixel size})$ is 10 (100-μm particles, 10-μm pixels). This gives approximate maximum errors in Cx of about 7.5%, in S^{QP} of about 12.5% (excluding the highly angular volcanic sand particles), and in AR of 15%. If the distribution of shapes by particle volume, rather than by number of particles, is considered, the effect of this error on the data is minimized. With improvements in computing power, memory, and optical technologies, future image-based systems will be able to analyze higher-resolution images, thus minimizing this error.

Database of Sand Shapes and Sizes

Samples of 36 different sands that have been used in laboratory research were analyzed using the QICPIC system, as listed in Table 2. Many of these sands are considered reference sands, and a literature review was carried out to assess how the morphologies of these sands have been qualitatively described in prior research. It would be impossible to include every reference to each of the sands considered, rather the review aimed to get representative descriptions of each sand, focusing primarily on peer-reviewed papers in international journals. There is not a consensus on the morphologies of even sands commonly considered to be standard, for example, Fontainebleau Sand has been described as angular, subangular, subrounded, and rounded and Toyoura Sand has been considered rounded, subangular, and subrounded by different researchers. The variations in description may be a consequence of real variations in morphology in heterogeneous natural deposits, or the sand morphologies may have evolved during testing. However, there is a real potential for inconsistency in the description to be a consequence of the subjective nature of the descriptors used. This uncertainty is unsatisfactory, because many studies have shown the mechanical response of sands to be sensitive to particle shape.

For each of the sands considered and tested in this study, the qualitative shape description was made using microscopy and visual examination, as listed in Table 2. In most cases, this description is in broad agreement with prior published assessments of the particle morphology. For the QICPIC data, recognizing the limits on the resolution of the images obtained (10 μm/pixel), consideration was restricted to particles having a Feret minimum diameter that exceeded 100 μm.

Consideration was given to the selection of appropriate representative shape measures. The distribution can be plotted either in terms of a cumulative distribution by number of particles or by volume. The particle volume is estimated by rotating the particle silhouette through 360°. Where the shape data are plotted in terms of particle volume a preferential weighting is given to larger particles. From a geomechanics perspective, this is probably the best way to look at the data, because DEM simulations (Shire and O'Sullivan 2013) and microcomputed tomography scans on sand (Fonseca 2011) both show that larger particles tend to have a larger number of contacts with other particles, and therefore are likely to have a dominant influence on the material response. However, a shape distribution by number of particles tells us more about what is happening across the entirety of the granular material. Fig. 10 compares the shape (sphericity) density and cumulative distributions by volume and number of particles considering Toyoura Sand and Ube Masado Sand. Just as the d_{50} size is used to select a representative value of size for a given sand, representative shape values could be chosen to be the value corresponding to a 50% cumulative distribution. The shape at ${d_{50}}^{Fmin}$ was determined from the plot of average shape factor against particle size, with the ${d_{50}}^{Fmin}$ value being obtained from the cumulative volumetric distribution of the d^{Fmin} values. Considering the data illustrated in Fig. 10, there is not a significant difference between the two approaches for Toyoura Sand; however, such good agreement is not observed for all sands. Ube Masado Sand is a highly angular sand and the difference between the distributions by volume and number indicate that there is a variation in sphericity with size (and hence particle volume) for this material.

Three approaches were used to obtain the representative shape values given in Table 2, that is, the cumulative distribution by volume, the cumulative distribution by number, and the value associated with the median particle size (${d_{50}}^{Fmin}$). The resultant values are denoted Cx_{50} for convexity, ${S^{QP}}_{50}$ for sphericity, and AR_{50} for aspect ratio. The representative values obtained are depended, to some extent, on the method chosen to obtain them. Considering, as an example, Monterey Sand, the cumulative distribution by volume gave values of $Cx_{50} = 0.95$, ${S^{QP}}_{50} = 0.89$, and $AR_{50} = 0.72$, the cumulative distribution by number gave values of $Cx_{50} = 0.95$, ${S^{QP}}_{50} = 0.89$, and $AR_{50} = 0.75$, and the values corresponding to the

J. Geotech. Geoenviron. Eng. 2013.139:1290-1307.

Table 2. Analysis of Sands Using QICPIC Size and Shape Analyzer

	By number			For $d_{50}{}^{Fmin}$			By volume								Shape classification-microscopy/visual observation in current study	$d_{50}{}^{Fmin}$ (μm)
Sand	Cx_{50}	$S^{QP}{}_{50}$	AR_{50}	Cx_{50}	$S^{QP}{}_{50}$	AR_{50}	Cx_{50}	$S^{QP}{}_{50}$	AR_{50}	Cx_{10}/Cx_{90}	S_{10}/S_{90}	AR_{10}/AR_{90}	Classification	Sources		
Corundum Sand	0.98	0.94	0.92	0.98	0.93	0.89	0.98	0.94	0.92	0.98	0.94	0.78	Rounded	Tatsuoka et al. (2008)	Rounded	1,556
Glass Ballotini	0.95	0.95	0.93	0.95	0.94	0.92	0.95	0.95	0.94	0.98	0.97	0.93	Rounded	Cavarretta (2009)	Rounded	213
Badger	0.98	0.91	0.71	0.98	0.93	0.82	0.98	0.93	0.81	0.98	0.96	0.75	Rounded	Rouse et al. (2008)	Rounded	890
Albany Sand	0.94	0.90	0.73	0.95	0.90	0.75	0.95	0.90	0.76	0.96	0.93	0.7	Rounded	Tatsuoka et al. (2008) and Kongkitkul et al. (2008)	Rounded	350
Ottawa Sand (coarse)	0.97	0.92	0.78	0.97	0.92	0.80	0.98	0.92	0.79	0.98	0.95	0.73	Rounded	Tatsuoka et al. (2008), Cho et al. (2006) ($R = 0.9$), Hagarty et al. (1993), Been et al. (1987)	Rounded	785
													Rounded to subrounded	Loukidis and Salgado (2009), Alshibli et al. (2003), Robertson et al. (1995)		
Silver Leighton Buzzard Sand	0.96	0.89	0.73	0.96	0.89	0.76	0.96	0.89	0.74	0.96	0.92	0.68	Rounded	Konagai et al. (1992), Yoshida et al. (2004), Lings and Dietz (2004), Arthur and Menzies (1972)	Rounded	731
													Subrounded	Tejchman and Niemunis (2006), Hoque and Tatsuoka (2004), Kohata et al. (1997)		
Ottawa Sand (fine)	0.97	0.92	0.77	0.96	0.91	0.76	0.96	0.91	0.79	0.97	0.94	0.72	—	—	Rounded/ Subrounded	404

J. Geotech. Geoenviron. Eng. 2013.139:1290-1307.

Table 2. (*Continued.*)

Sand	By number			For $d_{50}{}^{F\min}$			By volume						Classification	Sources	Shape classification-microscopy/visual observation in current study	$d_{50}{}^{F\min}$ (μm)
	Cx_{50}	$S^{QP}{}_{50}$	AR_{50}	Cx_{50}	$S^{QP}{}_{50}$	AR_{50}	Cx_{50}	$S^{QP}{}_{50}$	AR_{50}	Cx_{10}/Cx_{90}	S_{10}/S_{90}	AR_{10}/AR_{90}				
Kansas River Sand	0.97	0.89	0.74	0.96	0.89	0.75	0.96	0.90	0.76	0.96	0.92	0.7	—	—	Subrounded	729
Hime Gravel	0.98	0.88	0.73	0.98	0.89	0.74	0.98	0.89	0.75	0.98	0.93	0.69	Rounded to subrounded	Kiyota et al. (2007)	Subrounded	2,060
													Subrounded	Tatsuoka et al. (2008), Hoque and Tatsuoka (2004), Kohata et al. (1997)		
													Rounded	Kongkitkul et al. (2008)		
Monterey Sand	0.95	0.89	0.72	0.95	0.89	0.75	0.95	0.89	0.75	0.96	0.92	0.69	Rounded	Cudmani and Osinov (2001)	Subrounded	525
													Rounded to subrounded	Tatsuoka et al. (2008), Saxena and Reddy (1989)		
													Subrounded	Been et al. (1987), Salvati and Anhdan (2008)		
Nevada Sand	0.92	0.91	0.76	0.93	0.90	0.77	0.93	0.91	0.77	0.95	0.93	0.73	Rounded to subrounded ($R = 0.6$)	Cho et al. (2006)	Subrounded	164
													Angular	Yamamuro et al. (2008)		
Saltwash	0.92	0.90	0.76	0.92	0.90	0.74	0.92	0.90	0.75	0.95	0.92	0.71	Subrounded	Alvarado Gutierrez (2007)	Subrounded	170
Sacramento River Sand	0.93	0.89	0.71	0.94	0.88	0.73	0.94	0.89	0.73	0.95	0.91	0.67	Subangular	Lee and Seed (1967)	Subangular	316
Ticino Sand	0.94	0.88	0.70	0.95	0.88	0.72	0.95	0.88	0.73	0.96	0.91	0.66	Subrounded ($R = 0.4$)	Cho et al. (2006), Been et al. (1987)	Subangular	585
													Subangular	Cudmani and Osinov (2001), Hoque and Tatsuoka (2004), Kohata et al. (1997)		

Table 2. (*Continued.*)

Sand	By number			For $d_{50}{}^{Fmin}$			By volume						Classification	Sources	Shape classification-microscopy/visual observation in current study	$d_{50}{}^{Fmin}$ (μm)
	Cx_{50}	$S^{QP}{}_{50}$	AR_{50}	Cx_{50}	$S^{QP}{}_{50}$	AR_{50}	Cx_{50}	$S^{QP}{}_{50}$	AR_{50}	Cx_{10}/Cx_{90}	S_{10}/S_{90}	AR_{10}/AR_{90}				
Fontainebleau	0.93	0.90	0.73	0.94	0.90	0.75	0.94	0.90	0.76	0.95	0.92	0.7	Rounded	Puech and Foray (2002), Georgiannou et al. (2008), Bolton et al. (1999)	Subangular	230
													Subrounded	Dano et al. (2004)		
													Subangular	Yang et al. (2010)		
													Angular	Delfosse-Ribay et al. (2006)		
Hawaii Sand	0.96	0.88	0.70	0.95	0.86	0.73	0.96	0.86	0.73	0.94	0.88	0.65	—	—	Subangular	1,338

Sand	By number			For $d_{50}{}^{Fmin}$			By volume						Classification	Sources	Shape classification-microscopy/visual observation in current study	$d_{50}{}^{Fmin}$ (μm)
	Cx_{50}	$S^{QP}{}_{50}$	AR_{50}	Cx_{50}	$S^{QP}{}_{50}$	AR_{50}	Cx_{50}	$S^{QP}{}_{50}$	AR_{50}	Cx_{10}/Cx_{90}	S_{10}/S_{90}	AR_{10}/AR_{90}				
Toyoura Sand	0.93	0.89	0.71	0.93	0.89	0.74	0.93	0.89	0.74	0.95	0.91	0.66	Rounded	Cudmani and Osinov (2001)	Subangular	228
													Subrounded to subangular	Alvarado Gutierrez (2007)		
													Subangular	Herle and Gudehus (1999), Hoque and Tatsuoka (2004), Kohata et al. (1997), Been et al. (1987)		
													Subangular to angular	Loukidis and Salgado (2009)		
													Angular	Konagai et al. (1992)		
Hostun Sand	0.93	0.87	0.69	0.93	0.87	0.72	0.94	0.87	0.72	0.94	0.89	0.66	Subangular	Herle and Gudehus (1999)	Subangular	375
													Angular to subangular	Sadek (2006)		
													Relatively angular	Tatsuoka et al. (2008)		

J. Geotech. Geoenviron. Eng. 2013.139:1290-1307.

Table 2. (*Continued.*)

Sand	By number			For $d_{50}{}^{F\min}$			By volume						Classification	Sources	Shape classification-microscopy/visual observation in current study	$d_{50}{}^{F\min}$ (μm)
	Cx_{50}	$S^{QP}{}_{50}$	AR_{50}	Cx_{50}	$S^{QP}{}_{50}$	AR_{50}	Cx_{50}	$S^{QP}{}_{50}$	AR_{50}	Cx_{10}/Cx_{90}	S_{10}/S_{90}	AR_{10}/AR_{90}				
Fraser River Sand	0.93	0.89	0.70	0.94	0.88	0.72	0.94	0.88	0.72	0.95	0.9	0.65	Angular to subrounded Subangular to subrounded Subrounded	Wijewickreme et al. (2005) Uthayakumar and Vaid (1998) Robertson et al. (2000)	Subangular	315
Reigate	0.93	0.89	0.73	0.94	0.89	0.75	0.94	0.89	0.75	0.95	0.92	0.7	Well-rounded to angular	Creswell and Barton (2003), Fonseca (2011)	Subangular	260
Castlegate Sand	0.93	0.90	0.75	0.93	0.90	0.76	0.93	0.90	0.76	0.95	0.91	0.71	Subangular	Plona and Cook (1995), Alvarado Gutierrez (2007)	Subangular	188
Crushed Balottini	0.94	0.89	0.72	0.95	0.85	0.66	0.96	0.86	0.68	0.95	0.9	0.61	—	—	Subangular	1,276
Silica #3 Sand	0.96	0.88	0.78	0.96	0.89	0.80	0.96	0.88	0.80	0.97	0.94	0.76	Subangular	Yasufuku and Hyde (1995), Hyodo et al. (2002)	Subangular	1,436
Thames Valley	0.92	0.90	0.72	0.93	0.89	0.74	0.93	0.90	0.75	0.94	0.91	0.69	Subrounded to subangular	Takahashi and Jardine (2007)	Subangular	230
Aio Sand	0.86	0.86	0.68	0.94	0.85	0.70	0.95	0.86	0.72	0.95	0.9	0.64	Angular Subangular	Puech and Foray (2002) Yasufuku and Hyde (1995), Hyodo et al. (2002)	Subangular	1,107
Silica #8 Sand	0.91	0.89	0.72	0.91	0.87	0.68	0.91	0.88	0.71	0.93	0.88	0.63	Relatively angular	Tatsuoka et al. (2008)	Subrounded	170
Chiibishi Sand	0.92	0.86	0.66	0.92	0.82	0.67	0.93	0.84	0.70	0.9	0.82	0.57	Angular	—	Angular	783
Silica #6 Sand	0.91	0.87	0.66	0.92	0.86	0.65	0.92	0.87	0.66	0.94	0.87	0.57	Relatively angular	Kongkitkul et al. (2008)	Angular	231
Ube Masado Sand	0.92	0.88	0.71	0.93	0.83	0.75	0.94	0.84	0.76	0.94	0.86	0.71	Angular	—	Angular	1,408
Crushed Granite	0.92	0.87	0.70	0.93	0.84	0.71	0.93	0.85	0.72	0.94	0.88	0.65	Angular	—	Angular	531
Georgia Natural Sand	0.92	0.87	0.70	0.92	0.85	0.72	0.93	0.86	0.72	0.94	0.89	0.66	Angular	Cho et al. (2006)	Angular	456

Table 2. (*Continued.*)

Sand	By number			For $d_{50}^{F\min}$			By volume					Classification	Sources	Shape classification-microscopy/visual observation in current study	$d_{50}^{F\min}$ (μm)
	Cx_{50}	$S^{QP}{}_{50}$	AR_{50}	Cx_{50}	$S^{QP}{}_{50}$	AR_{50}	Cx_{50}	$S^{QP}{}_{50}$	AR_{50}	Cx_{10}/Cx_{90}	S_{10}/S_{90}	AR_{10}/AR_{90}				
Shirasu Sand	0.87	0.87	0.71	0.93	0.85	0.70	0.93	0.86	0.73	0.91	0.87	0.64	Angular	Hyodo et al. (2002)	Angular	543
Blessington	0.91	0.89	0.73	0.93	0.88	0.70	0.93	0.89	0.71	0.94	0.89	0.64	Highly angular	—	Angular	248
Dog's Bay Sand	0.92	0.86	0.64	0.91	0.83	0.67	0.92	0.85	0.68	0.9	0.83	0.56	Angular	Yasufuku and Hyde (1995)	Angular	412
GA 39	0.91	0.90	0.72	0.91	0.90	0.76	0.91	0.90	0.75	0.94	0.91	0.71	—	—	Angular	111
Icelandic Basalt	0.90	0.88	0.72	0.94	0.87	0.76	0.93	0.87	0.76	0.91	0.89	0.71	—	—	Angular	453
Osorio Sand	0.91	0.89	0.72	0.92	0.87	0.69	0.93	0.88	0.70	0.94	0.89	0.63	Rounded	Consoli et al. (2010)	Angular	265

Fig. 10. Illustration of selection of representative shape value: comparing distribution of sphericity values by volume and number for Toyoura Sand and Ube Masado Sand: (a) frequency distribution; (b) cumulative distribution

$d_{50}{}^{F\min}$ were given by $Cx_{50} = 0.95$, $S^{QP}{}_{50} = 0.89$, and $AR_{50} = 0.75$. Reviewing the full dataset for all the approaches used, the values of convexity were between $Cx_{50}{}^{\min} = 0.85$ and $Cx_{50}{}^{\max} = 0.98$, the sphericity values were between $S^{QP}{}_{50}{}^{\max} = 0.94$ and $S^{QP}{}_{50}{}^{\min} = 0.82$, and the aspect ratio values ranged from $AR_{50}{}^{\min} = 0.64$ to $AR_{50}{}^{\max} = 0.94$. The maximum difference in the Cx values, comparing all three approaches was $\Delta Cx_{50}{}^{\max} = 0.06$ (for Shirasu Sand), similarly $\Delta S^{QP}{}_{50}{}^{\max} = 0.05$ (for Ube Masado Sand) and $\Delta AR_{50}{}^{\max} = 0.05$ (again for Ube Masado Sand). When compared with the range of possible values, these differences are significant as $\Delta Cx_{50}{}^{\max}/Cx_{50}{}^{\max} - Cx_{50}{}^{\min} = 0.48$, $\Delta S^{QP}{}_{50}{}^{\max}/S^{QP}{}_{50}{}^{\max} - S^{QP}{}_{50}{}^{\min} = 0.41$, and $\Delta AR_{50}{}^{\max}/AR_{50}{}^{\max} - AR_{50}{}^{\min} = 0.17$. The average values were smaller; $\Delta Cx_{50}{}^{\text{ave}} = 0.01$, $\Delta S^{QP}{}_{50}{}^{\text{ave}} = 0.01$, and $\Delta AR_{50}{}^{\text{ave}} = 0.02$, and these values are 9.3, 8.9, and 7.8% of the respective ranges of values.

It is difficult to establish a simple link between the qualitative descriptors of geometry and the QICPIC shape parameters. Fig. 11 summarizes the range and average values obtained for each qualitative shape descriptor. Although it is clear that as the particles become more angular each of these shape metrics decreases, the range of values associated with different qualitative descriptors overlaps, and therefore no clear mapping between the values of the shape measures and the qualitative descriptions can be established. The most consistent trend in the data was observed by plotting the

J. Geotech. Geoenviron. Eng. 2013.139:1290-1307.

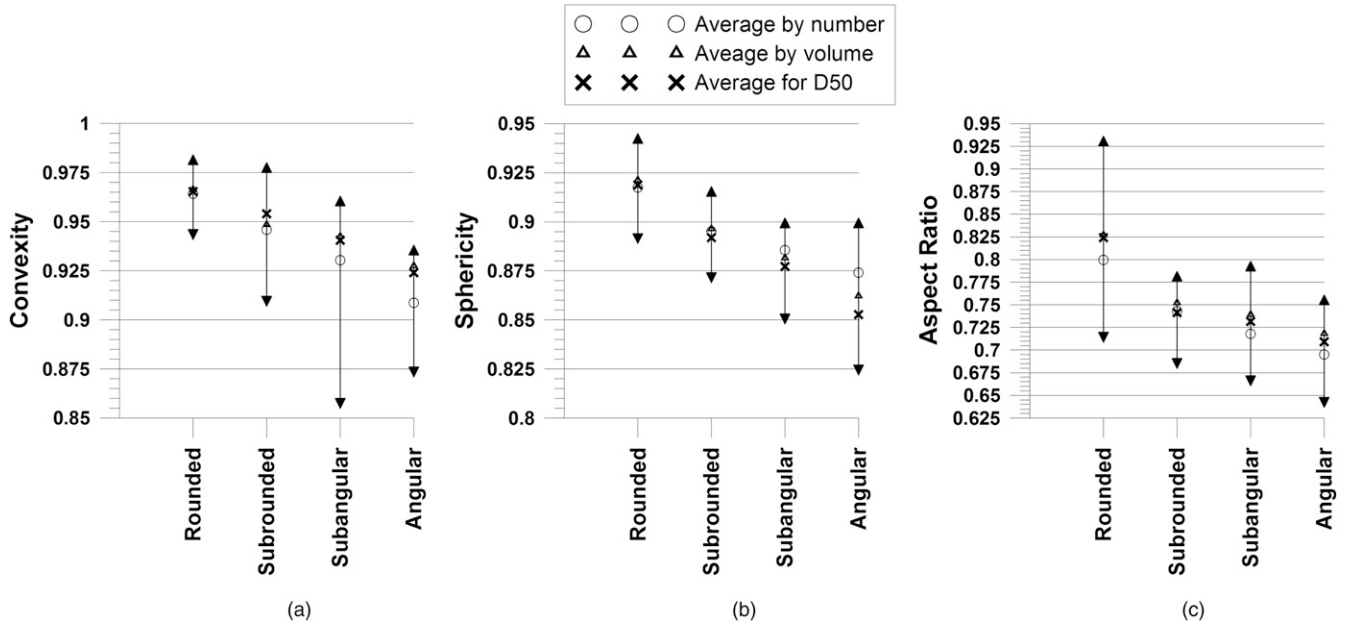

Fig. 11. Average and range of values by qualitative shape classification: (a) Cx_{50}; (b) S_{50}; (c) AR_{50}

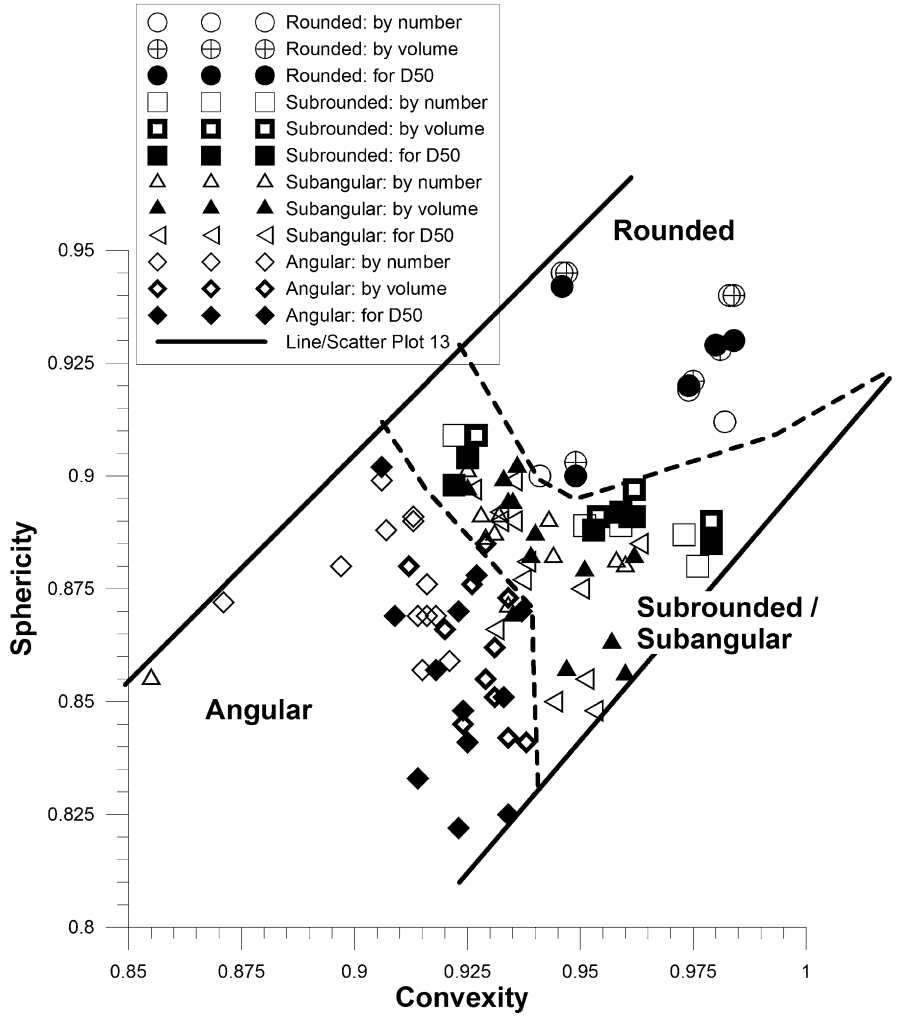

Fig. 12. Plot of sphericity values against convexity values for sands considered in Table 2, including representative values by number and volume and for d_{50}

J. Geotech. Geoenviron. Eng. 2013.139:1290-1307.

sphericity ($S^{QP}{}_{50}$) values against the convexity (Cx_{50}) values, as illustrated in Fig. 12. Here all three representative shape measures are simultaneously considered. Two straight lines can be drawn (by eye), defining the limiting combinations of representative values of sphericity and convexity that were observed for the sands considered. Tentative lines dividing the dataset into zones associated with the different qualitative descriptors have been drawn on this chart; the location of these lines is obviously subjective. Rounded particles have relatively high values of both sphericity and convexity, and angular particles have relatively low values of both sphericity and convexity. The division between the subangular and subrounded classifications is not clear; in general, these particles have combined sphericity and convexity values that are intermediate between the angular and rounded particles, and therefore we did not subdivide these categories in Fig. 12.

The correlation in Fig. 12 is somewhat clouded by the variation in the representative values for a given sand, depending on whether the values are selected from the cumulative distribution by number, volume, or for the $d_{50}{}^{F\min}$ size. Fig. 13 relates the Cx_{50} and $S^{QP}{}_{50}$ values from the volumetric shape distributions with the qualitative shape factors (as previously noted, these are probably the most representative values). As before, straight lines defining the limits of the Cx_{50} and $S^{QP}{}_{50}$ values observed were identified by visual observation. Tentative straight lines are drawn dividing the data into regions of combinations of sphericity and convexity for angular, subangular, subrounded, and rounded particles. Here subrounded values clearly lie closer to rounded values than subangular values, and therefore we considered these two as separate categories. The subrounded classification shows the most scatter.

To facilitate direct comparison with Fig. 13, Fig. 14(a) illustrates the $S^{QP}{}_{50}$ values plotted against the AR_{50} values, whereas Fig. 14(b) illustrates the AR_{50} values plotted against the Cx_{50} values. There is a weak linear correlation between the $S^{QP}{}_{50}$ and AR_{50} values, with an R^2 value of 0.49; however, although the general trend is for the AR_{50} values to increase as the Cx_{50} values increase, these values are even more poorly correlated with an R^2 value of only 0.22.

The range of shape values encountered for a given material can be appreciated by consideration of the extremes of the cumulative distribution plot, that is, the ratios Cx_{10}/Cx_{90}, where 90% of the particles have a convexity that is smaller than Cx_{90} and 10% of the particles have a convexity that is smaller than Cx_{10}. In a similar manner, values for $S^{QP}{}_{10}/S^{QP}{}_{90}$ and AR_{10}/AR_{90} can be found for the sphericity and aspect ratio data, respectively, and these values are given for all the sands in Table 2. Histograms summarizing the range of variations are given in Fig. 15; in comparison with the convexity and sphericity data, there is a wide variation in aspect ratio values for all the sands. The Cx values exhibit a smaller amount of variation than the S^{QP} values.

Any empirical correlation, whether graphical or analytical, depends on availability of a finite amount of experimental data. The complexity of the relationships motivated a graphical correlation by zones. To minimize the risk of misrepresenting the nature of the correlation, the raw data are clearly presented in Figs. 12 and 13.

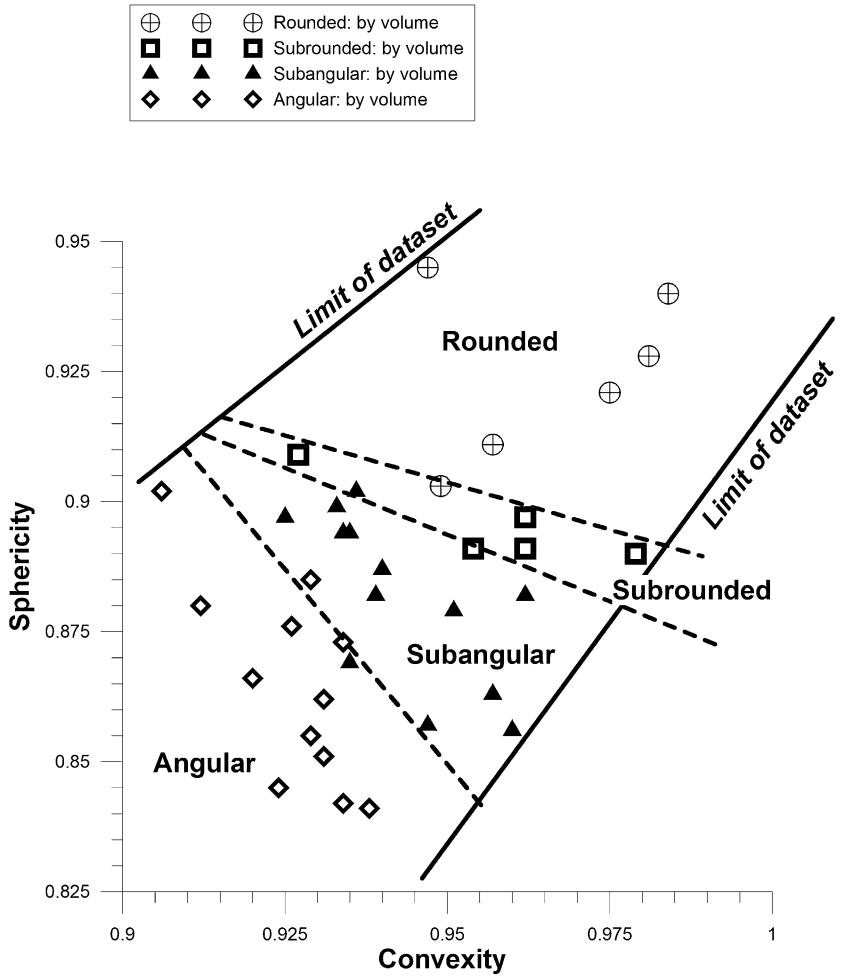

Fig. 13. Plot of sphericity versus convexity considering representative values by volume only

J. Geotech. Geoenviron. Eng. 2013.139:1290-1307.

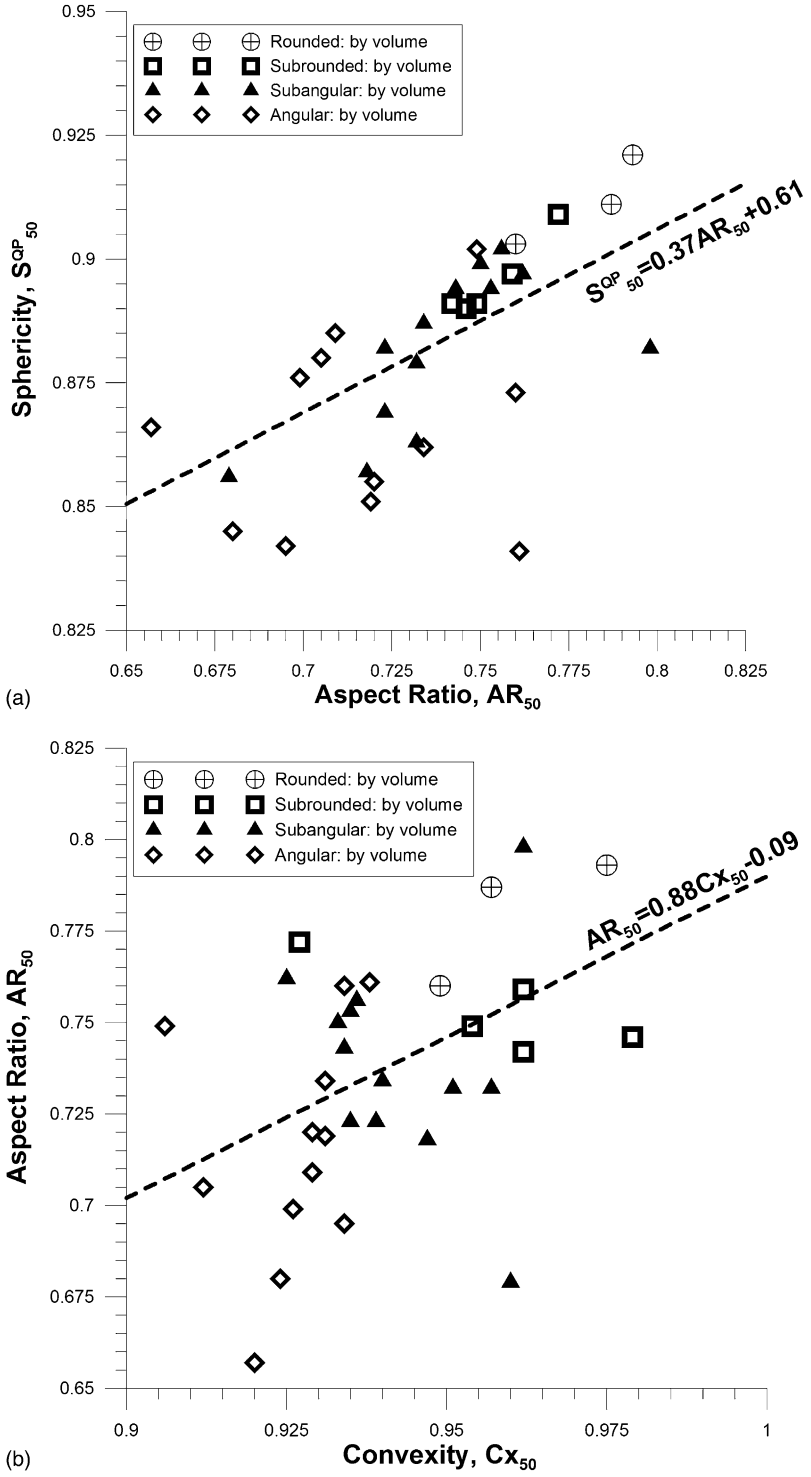

Fig. 14. (a) Plot of sphericity versus aspect ratio; (b) plot of aspect ratio versus convexity; in both cases, representative shape values (Cx_{50}, S_{50}, and AR_{50}) selected by volume are considered

The raw data are also provided in Table 2 to enable future alternative interpretations of the dataset.

Conclusions

Particle morphology is known to influence sand response; however, sand shape is typically qualitatively described. The subjective nature of this approach was highlighted by considering 36 laboratory sands and identifying inconsistencies in the shape classifications assigned to these sands in the literature.

A pragmatic approach to quantify particle morphology objectively using digitized images that has potential for a broad applicability has been critically analyzed. This approach uses binary images, and both size and shape can be quantified at the same time. Of the available size measures, the Feret minimum diameter was

J. Geotech. Geoenviron. Eng. 2013.139:1290-1307.

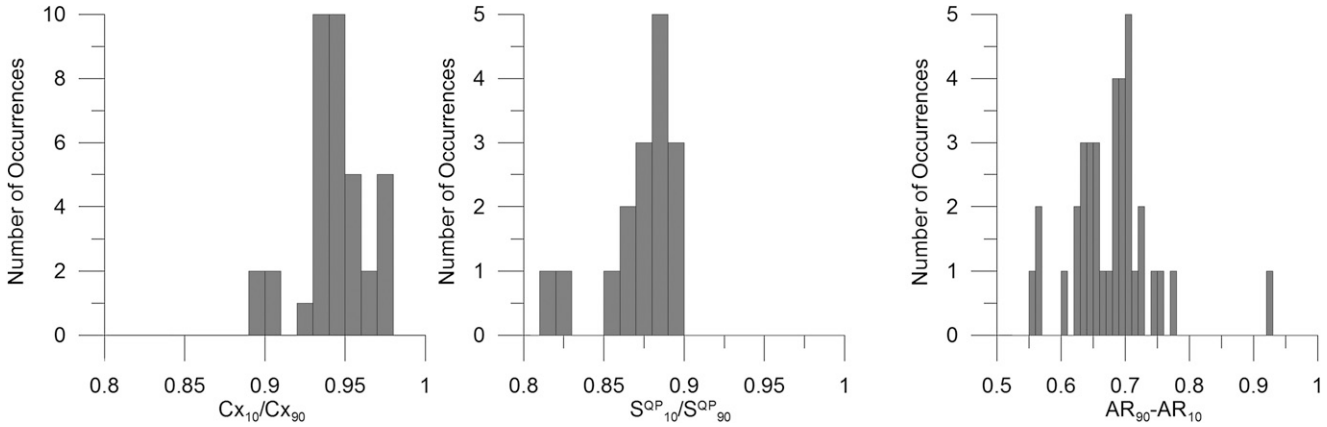

Fig. 15. Histograms illustrating the range of shape variations encountered in the dataset

shown to give the best approximation to the sieve method that is typically used to measure particle size.

Shape is characterized by applying simple formulas to get three measures, that is, convexity, sphericity, and aspect ratio. Although the data presented were collected using the QICPIC system, these three shape measures can be calculated easily from digital images obtained from other means, and therefore the findings are not restricted to use of this system. Notably, the approach avoids the evaluation of roundness, which is a scale-dependent parameter.

To enable a clear understanding of the new measures, they were applied to the widely used standard reference chart proposed by Krumbein and Sloss (1963) and Power's chart (1953). The QICPIC sphericity (S^{QP}) tends to increase with increasing sphericity, as calculated from Krumbein and Sloss (S^{KS}); however, the S^{KS} values do not simply correlate with either roundness or sphericity, as defined by Krumbein and Sloss. There is a clear tendency for both convexity and sphericity to increase as particles transition from being angular to rounded according to Power's graphical classification.

The comparison with existing methods was supplemented with a critical analysis of the method itself to highlight the limitations of its applicability. The binary images must have a sufficiently high resolution so that the Feret minimum diameter is greater than 10 times the pixel size.

Quantitative analysis of the database of 36 sands further contextualized the proposed method. Convexity, sphericity, and aspect ratio values for a number of commonly used research sands have been provided. In agreement with the analysis of Powers' chart, angular particles tend to have the lowest combined values of convexity and sphericity, whereas rounded particles have the highest combined values. The dataset was used to develop empirical, graphical relationships between the values of convexity and sphericity and the qualitative shape measures (i.e., angular, subangular, subrounded, and rounded).

Acknowledgments

The authors acknowledge the support of a number of academics from other institutions who provided sand samples to develop the database presented in Table 2. These included M. Bolton, University of Cambridge; R. Kuwano, University of Tokyo; E. Ibraim, University of Bristol; and M. Riemer, University of Berkeley. The QICPIC apparatus was funded by the EPSRC (Grant No. EP/F068778/1).

References

Abbireddy, C. O. R., and Clayton, C. R. I. (2009). "A review of modern particle sizing methods." *Proc., Instit. Civil Eng. Geotech. Eng.*, 162(4), 193–201.

Allen, T. (1997). *Particle size measurement. Vol.1: Powder sampling and particle size measurement*, 5th Ed., Chapman & Hall, London.

Alshibli, K. A., and Alsaleh, M. I. (2004). "Characterizing surface roughness and shape of sands using digital microscopy." *J. Comput. Civ. Eng.*, 18(1), 36–45.

Alshibli, K. A., Batiste, S. N., and Sture, S. (2003). "Strain localization in sand: Plane strain versus triaxial compression." *J. Geotech. Geoenviron. Eng.*, 129(6), 483–494.

Alvarado Gutierrez, G. (2007). "Influence of late cementation on the behaviour of reservoir sands." Ph.D. thesis, Imperial College London, London.

Arthur, J. R. F., and Menzies, B. K. (1972). "Inherent anisotropy in a sand." *Geotechnique*, 22(1), 115–128.

ASTM. (1990). "Description and identification of Soils (visual-manual procedure)." *D2488*, West Conshohocken, PA.

Barrett, P. J. (1980). "The shape of rocks particles, a critical review." *Sedimentology*, 27(3), 291–303.

Been, K., Jefferies, M. G., Crooks, J. H. A., and Rothenburg, L. (1987). "The cone penetration test in sands: Part II, general inference of state." *Geotechnique*, 37(3), 285–299.

Bolton, M. D., et al. (1999). "Centrifuge cone penetration tests in sand." *Geotechnique*, 49(4), 543–552.

Bowman, E., Soga, K., and Drummond, W. (2001). "Particle shape characterization using Fourier descriptor analysis." *Geotechnique*, 51(6), 545–554.

British Standards Institute. (1997). "Tests for geometrical properties of aggregates. Part 1: Determination of particle size distribution—Sieving method." *BS EN 933-1:1997*, London.

Cavarretta, I. (2009). "The influence of particle characteristics on the engineering behaviour of granular materials." Ph.D. thesis, Dept. Civil and Environmental Engineering, Imperial College London, London.

Cavarretta, I., O'Sullivan, C., and Coop, M. (2010). "The influence of particle characteristics on the behaviour of coarse grained soils." *Geotechnique*, 60(6), 413–423.

Chan, K. S. (2007). "The influence of particle shape on the behaviour of an ideal soil." M.Sc. dissertation, Dept. Civil and Environmental Engineering, Imperial College London, London.

Cho, G. C., Dodds, J., and Santamarina, J. C. (2006). "Particle shape effects on packing density, stiffness, and strength: Natural and crushed sands." *J. Geotech. Geoenviron. Eng.*, 132(5), 591–602.

Clark, M. W. (1981). "Quantitative shape analysis: A review." *Math. Geol.*, 13(4), 303–320.

Clayton, C. R. I., Xu, M., and Bloodworth, A. (2006). "A laboratory study of the development of earth pressures behind integral bridge abutments." *Geotechnique*, 56(8), 561–572.

J. Geotech. Geoenviron. Eng. 2013.139:1290-1307.

Consoli, N. C., Cruz, R. C., Floss, M. F., and Festugato, L. (2010). "Parameters controlling tensile and compressive strength of artificially cemented sand." *J. Geotech. Geoenviron. Eng.*, 136(5), 759–763.
Cresswell, A. W., and Barton, M. E. (2003). "Direct shear tests on an uncemented, and a very slightly cemented, locked sand." *Quart. J. Eng. Geol. Hydrogeol.*, 36(2), 119–132.
Cudmani, R., and Osinov, V. A. (2001). "The cavity expansion problem for the interpretation of cone penetration and pressuremeter tests." *Can. Geotech. J.*, 38(3), 622–636.
Dano, C., Hicher, P.-Y., and Tailliez, S. (2004). "Engineering properties of grouted sands." *J. Geotech. Geoenviron. Eng.*, 130(3), 328–338.
Delfosse-Ribay, E., Djeran-Maigre, I., Cabrillac, R., and Gouvenot, D. (2006). "Factors affecting the creep behavior of grouted Sand." *J. Geotech. Geoenviron. Eng.*, 132(4), 488–500.
Fonseca, J. (2011). "The evolution of morphology and fabric of a sand during shearing." Ph.D. thesis, Dept. Civil Engineering, Imperial College London, London.
Georgiannou, V. N., Tsomokos, A., and Stavrou, K. (2008). "Monotonic and cyclic behaviour of sand under torsional loading." *Geotechnique*, 58(2), 113–124.
Hagerty, M. M., Hite, D. R., Ullrich, C. R., and Hagerty, D. J. (1993). "One-dimensional high-pressure compression of granular media." *J. Geotech. Geoenviron. Eng.*, 119(1), 1–18.
Hamlin, S. (2009). "Particle size and shape of volcanic soils." M.Sc. dissertation, Dept. of Civil and Environmental Engineering, Imperial College London, London.
Herle, I., and Gudehus, G. (1999). "Determination of parameters of hypoplastic constitutive model from properties of grain assemblies." *Mech. Cohes.-Frict. Mater.*, 4(5), 461–486.
Holtz, R. D., and Kovacs, W. D. (1981). *An introduction to geotechnical engineering*, Prentice Hall, Englewood Cliffs, NJ.
Hoque, E., and Tatsuoka, F. (2004). "Effects of stress ratio on small-strain stiffness during triaxial shearing." *Geotechnique*, 54(7), 429–439.
Hyodo, M., Nakata, Y., Kuwajima, K., Yoshimoto, N., and Kato, Y. (2002). "Effect of fines and crushability on liquefaction of volcanic soil 'Shirasu'." *Proc., 12th (2002) Int. Offshore and Polar Eng. Conf.*, International Society of Offshore and Polar Engineers, Kitajyushu, Japan, 52–535.
ISO. (2008). "Representation of results of particle size analysis—Part 6: Descriptive and quantitative representation of particle shape and morphology." *ISO 9276-6:2008*, Geneva.
Joudi, A. (2008). "A reassessment of standard laboratory sands." M.Sc. dissertation, Imperial College London, London.
Kenney, T. C., and Lau, D. (1985). "Internal stability of granular filters." *Can. Geotech. J.*, 22(2), 215–225.
Kiyota, T., De Silva, L. I. N., Sato, T., and Koseki, J. (2007). "Small strain deformation characteristics of granular materials in torsional shear and triaxial tests with local deformation measurements." *Soil Stress-Strain Behavior: Measurement, Modeling and Analysis*. Springer, Dordrecht, Netherlands, 557–566.
Kohata, Y., et al. (1997). "Modelling the non-linear deformation properties of stiff geomaterials." *Geotechnique*, 47(3), 563–580.
Konagai, K., Tamura, C., Rangelow, P., and Matsushima, T. (1992). "Laser-aided tomography: A tool for visualization of changes in the fabric of granular assemblage." *Struct. Eng./Earthq. Eng.*, 9(3), 193–20.
Kongkitkul, W., et al. (2008). "Modelling and simulation of rate-dependent stress-strain behaviour of granular materials in shear." *Soils Found.*, 48(2), 175–194.
Krumbein, W. C., and Sloss, L. L. (1963). *Stratigraphy and sedimentation*, 2nd Ed., Freeman, San Francisco.
Labinski, E. (2011). "The influence of digital image resolution on the quantification of sand particle morphology." M.Eng. thesis, Dept. of Civil and Environmental Engineering, Imperial College London, London.
Lee, K. L., and Seed, H. B. (1967). "Drained strength characteristics of sands." *J. Soil Mech. and Found. Div.*, 93(6), 117–141.
Lings, M. L., and Dietz, M. S. (2004). "An improved direct shear apparatus for sand." *Geotechnique*, 54(4), 245–256.
Loukidis, D., and Salgado, R. (2009). "Modeling sand response using two-surface plasticity." *Comput. Geotech.*, 36(1–2), 166–186.
MacLeod, N. (2002). "Geometric morphometrics and geological shape-classification systems." *Earth Sci. Rev.*, 59(1), 27–47.
MathWorks. (2011). "MATLAB Image Processing Toolbox." ⟨http://www.mathworks.com/products/image/⟩.
McCave, I. N., and Syvitski, J. P. M. (1991) "Principles and methods of geological particle size analysis." *Principles, methods, and application of particle size analysis*, J. P. M. Syvitski, ed., Cambridge University Press, Cambridge, U.K, 3–21.
Mitchell, J. K., and Soga, K. (2005) *Fundamentals of soil behavior*, Wiley, New York.
Pestana, J. M., and Salvati, L. A. (2006). "Small strain behavior of granular soils: I. Model for cemented and uncemented sands and gravels." *J. Geotech. Geoenviron. Eng.*, 132(8), 1071–1081.
Pestana, J. M., and Whittle, A. J. (1995). "Compression model for cohesionless soils." *Geotechnique*, 45(4), 611–631.
Plona, T. J., and Cook, J. M. (1995). "Effects of stress cycles on static and dynamic Young's moduli in Castlegate sandstone." *Proc., 35th Rock Mechanics Symp.*, Daemen and Schultz, eds., Balkema, Rotterdam, Netherlands.
Powers, M. C. (1953). "A new roundness scale for sedimentary particles." *J. Sediment. Res.*, 23(2), 117–119.
Puech, A., and Foray, P. (2002). "Refined model for interpreting shallow penetration CPTs in sands." *Proc., 2002 Offshore Technol. Conf.*, OTC, 14275.
Rhodes, M. (2000). *Introduction to particle technology*, Wiley, Chichester, U.K.
Robertson, P. K., et al. (2000). "The Canadian liquefaction experiment: An overview." *Can. Geotech. J.*, 37(3), 499–504.
Robertson, P. K., Sasitharan, S., Cunning, J. C., and Sego, D. C. (1995). "Shear-wave velocity to evaluate in-situ state of Ottawa sand." *J. Geotech. Eng.*, 121(3), 262–273.
Rouse, P. C., Fannin, R. J., and Shuttle, D. A. (2008). "Influence of roundness on the void ratio and strength of uniform sand." *Geotechnique*, 58(3), 227–231.
Sadek, T. (2006). "The multi-axial behaviour and elastic stiffness of Hostun sand." Ph.D. thesis, Dept. of Civil Engineering, Univ. of Bristol, Bristol, U.K.
Salvati, L. A., and Anhdan, L. Q. (2008). "Rate-dependent response of dense sand in cyclic triaxial tests." *Soils Found.*, 48(3), 447–451.
Saxena, S. K., and Reddy, K. R. (1989). "Dynamic moduli and damping ratios for Monterey No. 0 sand by resonant column tests." *Soils Found.*, 29(2), 37–51.
Schneider, C. A., Rasband, W. S., and Eliceiri, K. W. (2012). "NIH Image to ImageJ: 25 years of image analysis." *Nature Methods*, 9, 671–675.
Shire, T., and O'Sullivan, C. (2013). "Micromechanical assessment of filter stability." *Acta Geotech*, 8(1), 81–90.
Sukumaran, B., and Ashmawy, A. (2001). "Quantitative characterization of discrete particles." *Geotechnique*, 51(7), 619–627.
Sympatec. (2008). *Windox—operating instructions release 5.4.1.0*, Sympatec, Clausthal-Zellerfeld, Germany.
Takahashi, A., and Jardine, R. J. (2007). "Assessment of standard research sand for laboratory testing." *Quart. J. Eng. Geol. Hydrogeol.*, 40(1), 93–103.
Tatsuoka, F., Di Benedetto, H., Enomoto, T., Kawabe, S., and Kongkitkul, W. (2008). "Various viscosity types of geomaterials in shear and their mathematical expression." *Soils Found.*, 48(1), 41–60.
Tejchman, J., and Niemunis, A. (2006). "FE-studies on shear localization in an anistropic micro-polar hypoplastic granular material." *Granul. Matter*, 8(3–4), 205–220.
Uthayakumar, M., and Vaid, Y. P. (1998). "Static liquefaction of sands under multiaxial loading." *Can. Geotech. J.*, 35(2), 273–283.
Wadell, H. A. (1932). "Volume, shape, and roundness of rock particles." *J. Geol.*, 40(5), 1074–1106.
White, D. J. (2003). "PSD measurement using the single particle optical sizing (SPOS) method." *Geotechnique*, 53(3), 317–326.
Wijewickreme, D., Sriskandakumar, S., and Byrne, P. (2005). "Cyclic loading response of loose air-pluviated Fraser River sand for validation of numerical models simulating centrifuge tests." *Can. Geotech. J.*, 42(2), 550–561.
Witt, W., Köhler, U., and List, J. (2004). "Direct imaging of very fast particles opens the application of the powerful (dry) dispersion for size and shape characterization." *Proc., PARTEC 2004*, Nürnberg, Germany.

J. Geotech. Geoenviron. Eng. 2013.139:1290-1307.

Yamamuro, J. A., Wood, F. M., and Lade, P. V. (2008). "Effect of depositional method on the microstructure of silty sand." *Can. Geotech. J.*, 45(11), 1538–1555.

Yang, J. (2006). "Influence zone for end bearing of piles in sand." *J. Geotech. Geoenviron. Eng.*, 132(9), 1229–1237.

Yang, Z. X., Jardine, R. J., Zhun, B. T., Foray, P., and Tsuha, C. H. C. (2010). "Sand grain crushing and interface shearing during displacement pile installation in sand." *Geotechnique*, 60(6), 469–482.

Yasufuku, N., and Hyde, A. F. L. (1995). "Pile end-bearing capacity in crushable sands." *Geotechnique*, 45(4), 663–676.

Yoshida, S., Johnson, H. D., Pye, K., and Dixon, R. J. (2004). "Transgressive changes from tidal estuarine to marine embayment depositional systems." *AAPG Bull.*, 88(10), 1433–1460.

Youd, T. (1972). "Factors controlling maximum and minimum densities of sands." *Evaluation of relative density and its role in geotechnical projects involving cohesionless soils*, E. T. Selig and R. S. Ladd, eds., ASTM, West Conshohoken, PA, 98–112.

Zeiss. (2007). "Digital imaging—Topography." ⟨http://www.zeiss.co.uk/4125681F004E2140/EmbedTitelIntern/AxioVisionforMaterials/$File/AxioVision_Materials.pdf⟩ (Nov. 1, 2007).